

## Thermal Surface Properties of CFC- NB31

D. Hildebrandt, J. Boscarý<sup>1</sup>, M. Rödíg<sup>2</sup>,

*EURATOM Association Max-Planck-Institut für Plasmaphysik, Teilinstitut Greifswald,  
Wendelsteinstr.1, D-17491 Greifswald, Germany*

<sup>1</sup> *EURATOM Association Max-Planck-Institut für Plasmaphysik  
Boltzmannstr.2, D-80805 Munich, Germany*

<sup>2</sup> *Forschungszentrum Jülich GmbH, EURATOM Association  
P.O.Box 1913, D-52425 Jülich, Germany*

### 1. Introduction

The carbon reinforced fiber carbon CFC-NB31 has been selected to shield the target elements of the Wendelstein 7-X stellarator. The water-cooled targets are designed to withstand stationary heat fluxes up to 10 MW/m<sup>2</sup>. Surface temperature measurements by infrared thermography are planned to survey the power fluxes arriving at these plates.

Experiments have been performed to study the relation between the measured surface temperature and the incident heat flux density.

In the first experiment CFC-NB31 specimens have been heated by light pulses from a diode laser and the surface temperature excursion has been measured by an IR-camera. The results are compared with an analytic solution of the three-dimensional heat diffusion equation [1].

Secondly, W7-X pre-series target elements with active water cooling have been thermally examined in the JUDITH device [2] to simulate operating conditions in W7-X. Their surface was viewed by an IR camera during heating by a 120 KeV electron beam. In this case the measured temperature values are compared to results from the finite element code ANSYS.

### 2. Results

#### 2.1. Laser Heating

NB31 specimens of 65x28x12 mm<sup>3</sup> size have been irradiated by light pulses ( $\lambda = 808$  nm) from a diode laser with normal incidence. The surface temperature excursion was measured by an IR camera (256x320 pixels) operating in the wavelength region between 3-5  $\mu$ m. Using microscopic lenses the spatial resolution was improved to up to 30  $\mu$ m. The thermal images have been taken with frame rates of 315 Hz (full frame) or up to 10 kHz at reduced image size. Before the heat pulse the sample had an uniform temperature of about 307 K. The apparent temperature distribution seen in Fig.1(left) results from a variation of the emissivity. The fiber bundles (bright) have an emissivity up to a value of 0,98 and the filler material (dark regions) of about 0,87. The mean area value is  $\epsilon = 0,93$ .

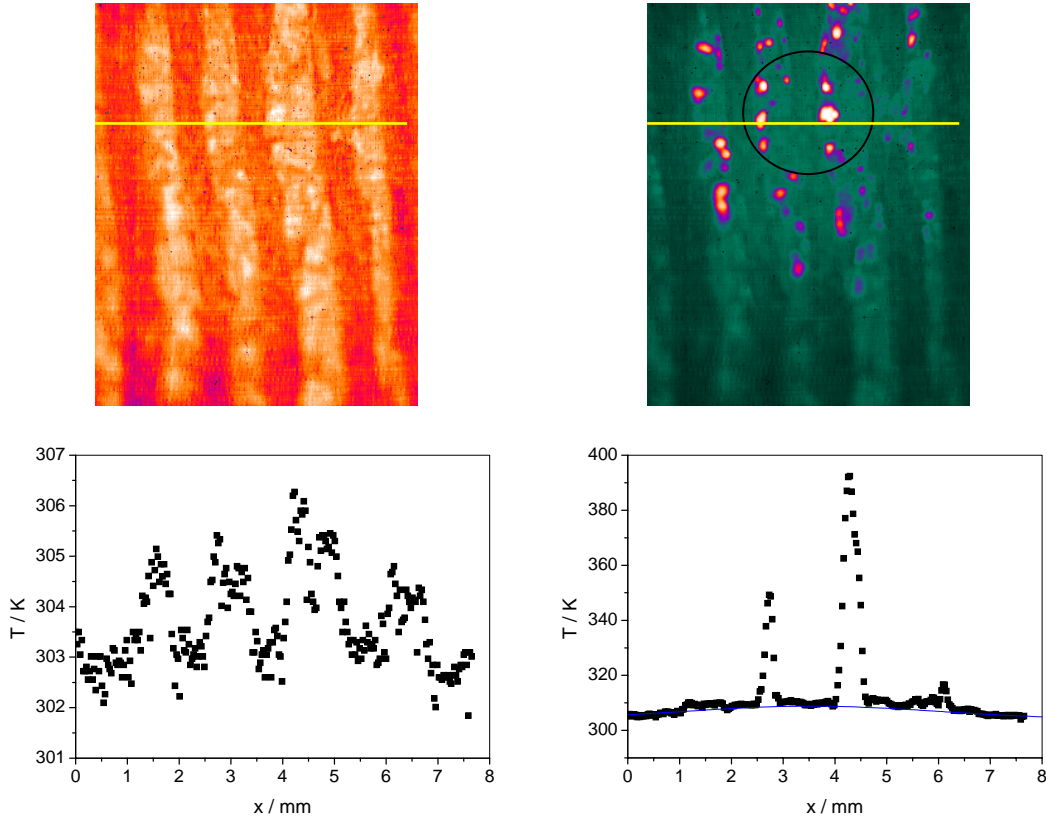


Fig.1: Thermal images before (left) and during (right) a laser heat pulse  $P_0 = 0,4 \text{ MW/m}^2$ ,  $\tau_p = 100 \text{ ms}$ ,  $\sigma = 2,45 \text{ mm}$ . Bottom: Apparent temperature (without  $\varepsilon$  correction) along the marked lines. The solid blue curve is calculated (see text).

The temperature distribution during the heat pulse reveals that some parts in the fiber bundles have a higher thermal resistance causing an enhanced local surface temperature. The solid blue curve is  $T = T_\tau * \exp((x - x_o)/2\sigma^2)$  with  $T_\tau$  calculated from equation (1) for  $t = \tau_p$  using the thermal parameters of the bulk material at room temperature ( $\rho = 2*10^3 \text{ kg/m}^3$ ,  $c_p = 770 \text{ J/kgK}$ ,  $\lambda_x = 300 \text{ W/Km}$ ,  $\lambda_y=110 \text{ W/Km}$  and  $\lambda_z = 90 \text{ W/Km}$ ).

The temporal evolution of the measured surface temperature at two different positions with different thermal resistance (hot spot in the fiber bundle and filler material) is shown in Fig.2. In order to simulate measurements with an ordinary spatial resolution the pixel signals of the central spot area are combined and compared with the analytic solution (Eq.(1)).

$$T - T_o = \frac{\sqrt{2}}{\sqrt{\pi}} * \frac{\sigma * P_o}{\sqrt{\lambda_x * \lambda_{y,z}}} * \left[ \arctan \left( \sqrt{\frac{2\kappa_{y,z} * t}{\sigma^2}} \right) - \Theta(t - \tau_p) * \arctan \left( \sqrt{\frac{2\kappa_{y,z} * (t - \tau_p)}{\sigma^2}} \right) \right]$$

with  $\kappa = \lambda/\rho c_p$ ,  $P_0$  the heat flux density,  $\tau_p$  the pulse duration and  $\Theta$  the Heaviside function.

The averaged temperature increase (fig.2, right) exceeds the calculated value from Eq.(1) by

more than 100 % similar to that earlier observed with the CFC-material N11 at oblique light incidence [1]. This is due to some hot spots which significantly contribute to the averaged signal (fig.2, left). The temperature evolution in the hot regions can be well described by a simple layer model on top of the bulk [3, 4]. The temperature excursion is given by Eq. (2)

$$\Delta T = P_0/\alpha * [(1-\exp(-t/\tau)) - \Theta(t-\tau_p)*\exp(-(t-\tau_p)/\tau)] \quad (2)$$

with  $\tau = C_0/\alpha$ .  $1/\alpha$  is the thermal resistance of the layer plus the resistance of the contact between the layer and the bulk material and  $C_0 = c_p \rho d$  the thermal mass per unit area of the involved material ( $d$  represents the thickness). Taking  $\Delta T = 80$  K (see Fig.2, left)  $\alpha = 5$  kW/m<sup>2</sup>K is obtained and with  $\tau = 5$ ms as observed  $C_0$  is 25 J/m<sup>2</sup>K and  $d = 16$   $\mu$ m.

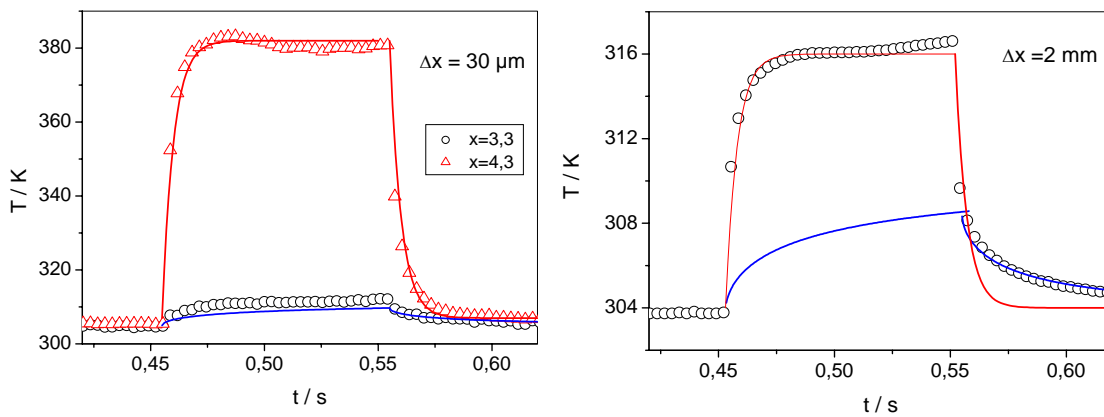


Fig.2.: Left: Temperature excursions measured with a spatial resolution of 30  $\mu$ m at  $x = 3,3$ m (filler material) and  $x = 4,3$  mm (hot spot in the fiber bundle) (see fig.1).

Right: Temporal evolution of an averaged temperature value obtained by combining the pixel signals from the central area of 2x2mm. The blue lines are derived from equation (1) and the red lines are calculated using equation (2) with  $\tau = 5$ ms.

The temporal evolution of the averaged temperature (see fig.2, right) can be well described by a combination of both models. Thus, the temperature response is dominated for short time intervals after power load change by the hot spots whereas later the time dependence of the temperature is in good agreement with Eq.(1) using the thermal bulk material parameters.

## 2.2. Electron beam heating

The NB31 tiles were heated with an electron beam of 1-2 mm diameter swept with an horizontal and vertical frequency of 40 kHz and 31 kHz, respectively. Fig.3 (left side) shows an IR picture of the surface of two adjacent tiles. The heated surface of 60mm x 50mm was viewed by an IR camera with temporal and spatial resolution of 0,5 s and 0,5 mm, respectively. The surface temperature is about 1100 <sup>0</sup>C and rather uniform (Fig.3, left side). It

is in good agreement with temperature values measured by thermocouples which were located 4 mm away from the surface and it agrees also with the predicted value of the finite element code ANSYS within 20 % using temperature dependent values of  $c_p$  and  $\lambda$ .

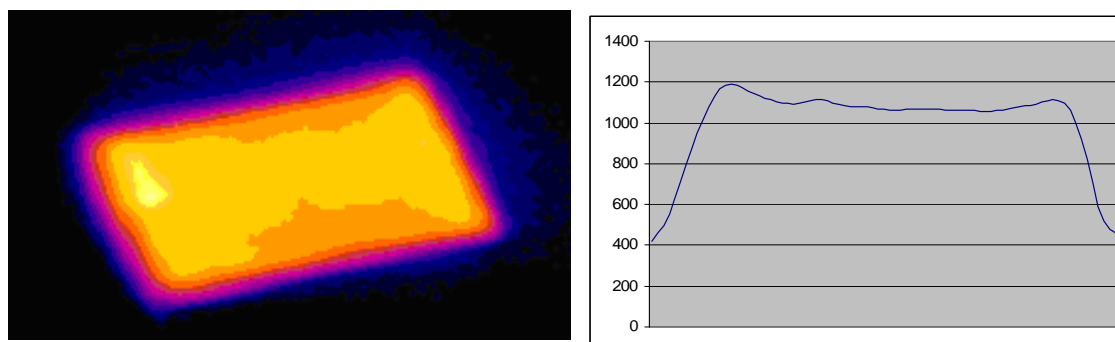


Fig.3 (left): IR-image of a W7-X pre-series target element heated by a scanned electron beam; averaged power flux density is 12,7 MW/m<sup>2</sup>; (right) Temperature values in °C along the marked line. Water cooling conditions are an inlet temperature of 20 °C and a flow rate of 34l / min.

### 3. Discussion

Whereas significant deviations of the surface temperature excursion between measured and calculated values by more than 100 % are observable during laser heating much better agreement is achieved by heating with accelerated electrons. As shown in Fig.1 and 2 the discrepancy at laser heating is caused by microscopic surface parts in the fiber bundles with a high thermal resistance to the underlying material. The thermal time constant of up to 5 ms indicates an involved material thickness of 10-20  $\mu\text{m}$  with poor thermal contact which can be an explanation for the different observations. While the energy of the laser is absorbed within this depth the electrons can penetrate through this material layer and leave the main portion of their energy at larger depths. In fact, the range of 120 keV electrons is about 100  $\mu\text{m}$  [5]. Another explanation is that surface material with extremely poor thermal contact is evaporated at high heat load as applied in the JUDITH device. Clarification is expected from heating experiments using ion beams prepared in the Ion Beam Test Facility at IPP-Garching.

### References

- [1] D. Hildebrandt et al., J. Nucl. Mater.337-339(2005), 1064
- [2] R. Duwe et al., Fusion Technology (1995), 356
- [3] P. Andrew et al., J. Nucl. Mater.337-339(2005), 99
- [4] E. Gauthier et al., J. Nucl. Mater.337-339(2005), 960
- [5] S. Schiller et al.: „Electron Beam Technology”, Berlin 1982